Am J Physiol Endocrinol Metab 315: E38–E51, 2018.
First published December 19, 2017; doi:10.1152/ajpendo.00227.2017.

RESEARCH ARTICLE

Different physiological roles of insulin receptors in mediating nutrient metabolism in zebrafish

Bin-Yuan Yang,[1,2]* Gang Zhai,[1]* Yu-Long Gong,[1,2]* Jing-Zhi Su,[1,2] Xu-Yan Peng,[1,2] Guo-Hui Shang,[1,2] Dong Han,[1,3] Jun-Yan Jin,[1] Hao-Kun Liu,[1] Zhen-Yu Du,[4] Zhan Yin,[1] and Shou-Qi Xie[1]

[1]*State Key Laboratory of Freshwater Ecology and Biotechnology, Institute of Hydrobiology, Chinese Academy of Sciences, Wuhan, China;* [2]*University of Chinese Academy of Sciences, Beijing, China;* [3]*Freshwater Aquaculture Collaborative Innovation Center of Hubei Province, Wuhan, China; and* [4]*Laboratory of Aquaculture Nutrition and Environmental Health, School of Life Sciences, East China Normal University, Shanghai, China*

Submitted 5 July 2017; accepted in final form 13 December 2017

Yang BY, Zhai G, Gong YL, Su JZ, Peng XY, Shang GH, Han D, Jin JY, Liu HK, Du ZY, Yin Z, Xie SQ. Different physiological roles of insulin receptors in mediating nutrient metabolism in zebrafish. *Am J Physiol Endocrinol Metab* 315: E38–E51, 2018. First published December 19, 2017; doi:10.1152/ajpendo.00227.2017.—Insulin, the most potent anabolic hormone, is critical for somatic growth and metabolism in vertebrates. Type 2 diabetes, which is the primary cause of hyperglycemia, results from an inability of insulin to signal glycolysis and gluconeogenesis. Our previous study showed that double knockout of *insulin receptor a* (*insra*) and *b* (*insrb*) caused β-cell hyperplasia and lethality from 5 to 16 days postfertilization (dpf) (Yang BY, Zhai G, Gong YL, Su JZ, Han D, Yin Z, Xie SQ. *Sci Bull (Beijing)* 62: 486–492, 2017). In this study, we characterized the physiological roles of Insra and Insrb, in somatic growth and fueling metabolism, respectively. A high-carbohydrate diet was provided for insulin receptor knockout zebrafish from 60 to 120 dpf to investigate phenotype inducement and amplification. We observed hyperglycemia in both *insra*−/− fish and *insrb*−/− fish. Impaired growth hormone signaling, increased visceral adiposity, and fatty liver were detected in *insrb*−/− fish, which are phenotypes similar to the lipodystrophy observed in mammals. More importantly, significantly diminished protein levels of P-PPARα, P-STAT5, and IGF-1 were also observed in *insrb*−/− fish. In *insra*−/− fish, we observed increased protein content and decreased lipid content of the whole body. Taken together, although Insra and Insrb show overlapping roles in mediating glucose metabolism through the insulin-signaling pathway, Insrb is more prone to promoting lipid catabolism and protein synthesis through activation of the growth hormone-signaling pathway, whereas Insra primarily acts to promote lipid synthesis via glucose utilization.

GH signaling; hyperglycemia; insulin receptors; lipid metabolism

INTRODUCTION

Insulin is well known as the most potent anabolic hormone. It plays a fundamental role in the regulation of somatic growth and metabolism of vertebrates (16). The insulin/insr interaction serves to amplify and diversify insulin action (28, 45). The major effects of insulin include stimulation of glucose utilization and synthesis of glycogen, lipids, and protein (8). Even mild impairment of insulin secretion may have a great impact on metabolic homeostasis. Decreased insulin secretion leads to increased food intake and weight gain (brain), decreased glucose uptake (muscle), decreased inhibition of glucose production (liver), and increased lipolysis (adipocytes) (22). However, there is a gap in our understanding of the precise function of insulin/insr pathway in the nutritional metabolism of teleosts.

The insulin receptor (INSR) belongs to the tyrosine kinase receptor subfamily, which is expressed at the cell surface as heterodimers and monomers (37). After binding to insulin, a conformational change is triggered that enables the receptor to bind ATP and activate INSR tyrosine kinases (20). Insulin receptor substrate proteins (IRS) are then phosphorylated as a critical node, leading to activation of downstream pathways of two other critical nodes, phosphatidylinositol 3-kinase (PI3K) and AKT/PKB, which control the metabolic action of insulin and regulate the expression of genes that mediate cell growth and differentiation (2, 51).

A thorough systematic study of INSR dysfunction in mice has been conducted (28). Briefly, depletion of Insr in mice resulted in only slight growth retardation at birth. After birth, glucose levels rose to 1,000-fold above normal upon feeding, which was followed by death from diabetic ketoacidosis (1, 21). Meanwhile, humans lacking INSR showed severe intrauterine growth retardation, failure to thrive, fasting hypoglycemia, postprandial hyperglycemia, and other insulin-resistant syndromes (11, 53, 58). The Cre-lox P system has been used to create a tissue-specific Insr knockout to clarify the role of Insr-mediated signaling in fueling homeostasis and to measure physiological effects in a tissue-specific manner (28). The lethal phenotype of Insr knockout made it difficult for a comprehensive understanding of insulin receptor function in tissues of adult mice, whereas the conditional ablation of Insr in the target tissue only allowed for a partial understanding of the effects of tissue-specific Insr knockout on whole body metabolism.

Mammals have two alternative splice variants of exon 11 from the *insr* gene after activation of insulin in tissues. However, the zebrafish genome was duplicated during evolution and there are two *insr* genes: *insra* and *insrb*, which share 68.3 and 65.1% sequence homology with human *INSR*, respectively

* B.-Y Yang, G. Zhai, and Y.-L Gong contributed equally to this work.

Address for reprint requests and other correspondence: D. Han, State Key Laboratory of Freshwater Ecology and Biotechnology, Institute of Hydrobiology, Chinese Academy of Sciences, Wuhan 430072, China (e-mail: hand21cn@ihb.ac.cn).

(54). Furthermore, these two individual zebrafish *insr* genes are 75.3% identical to each other in their primary sequence (54). Meanwhile, similar to the expression pattern of human INSRA and INSRB variants, *insra* and *insrb* are also expressed in insulin-secreting cells in zebrafish (60). Therefore, studying physiological roles of insulin could benefit from the functional analysis of Insra and Insrb.

We have established *insra*- and/or *insrb*-knockout models in zebrafish and have evaluated the effects of redundant and overlapping roles of these receptors during early development of zebrafish (60). Not surprisingly, a lethal phenotype was observed in the *insra* and *insrb* double knockout zebrafish before 16 days postfertilization (dpf), which was similar to results in *Insr* knockout mouse (1, 21) and humans with *INSR* mutations (11, 53, 58). However, despite higher glucose levels caused by the increased gluconeogenesis and decreased glycolysis in single and double knockout zebrafish at 3–5 dpf, the *insra* or *insrb* knockout zebrafish could survive, grow, and breed normally when they were fed with *Artemia salina*. Therefore, various *insr* knockout zebrafish lines offered an unrivaled model to explore the basal functions of insulin/insr signaling at adult stages.

Many studies of the two receptors in zebrafish embryonic stages have shown that Insra and Insrb have different, albeit somewhat overlapping, roles during early development (54). To further investigate the different roles of Insra and Insrb in somatic growth and fuel metabolism, we used individual *insr* knockout fish and comparatively analyzed the biological functions of each *insr* under the inducement and amplification of a high carbohydrate-diet condition (HCD).

Table 1. *The formulation and composition of the high-carbohydrate diet*

Ingredients	Content, %
Casein	33.00
Gelatin	2.00
Dextrin	24.00
Corn starch	24.00
Soybean oil	8.00
Vitamin premix	0.90
Choline chloride	0.10
Mineral premix	1.00
Monocalcium phosphate	2.50
Crystalline amino acid	
L-Ala	1.00
L-Arg	1.00
L-Asp	1.00
L-Gly	1.00
L-Lys	0.50
Proximate composition	
Moisture, %	13.50
Crude protein, %DM	36.32
Crude fat, %DM	5.50
Carbohydrate, %DM	41.42
Ash, %DM	3.26
Gross energy, kJ/g	20.67

Casien and crystalline amino acid (purity ≥98%) were imported from Sigma (St. Louis, MO). Gelatin was purchased from Tainjin Bodi Chemical Holding (Tianjin, China). Vitamin premix (mg/kg diet) contained the following: 100 tocopherol acetate, 25 sodium menadione bisulfate, 6.9 retinyl acetate, 0.05 cholecalciferol, 30 thiamin, 30 riboflavin, 20 pyridoxine, 0.1 cyanocobalamin, 200 nicotinic acid, 15 folic acid, 1,000 ascorbic acid, 500 inositol, 3 biotin, and 100 calcium pantothenate. Mineral premix (mg/kg diet) contained the following: 0.65 $CoCO_3$, 9 $CuSO_4$, 8.34 $FeSO_4 \cdot 7H_2O$, 0.5 KI, 22.85 $MnSO_4 \cdot H_2O$, 0.01 $NaSeO_3$, 14.3 $ZnSO_4 \cdot 7H_2O$, 400 NaCl, 1,860 $CaCO_3$, and 240 MgO, 240. Carbohydrate [%dry matter (DM)] = 100 − (crude protein + crude fat + crude ash).

MATERIALS AND METHODS

Ethics statement. The experimental fish were obtained from the Institute of Hydrobiology, Chinese Academy of Sciences (Wuhan, China). All animal experiments were conducted according to the *Guiding Principles for the Care and Use of Laboratory Animals* and were approved by the Institute of Hydrobiology, Chinese Academy of Sciences (Approval ID: IHB 2013724).

Establishing insra or insrb knockout lines. The *insra* or *insrb* knockout lines of zebrafish used in this study were described previously (60). Regions containing restriction enzyme sites for ACCI or Tsp45I were targeted for knockout in *insra*−/− or *insrb*−/− fish, respectively. Additionally, identification of the indigestive amplified fragment of the target region containing ACCI or Tsp45I from individual tail DNA was used for mutant screening. We established three genetic zebrafish groups for the experiments: *insra*−/−, *insrb*−/−, and control fish.

Experimental diets. A HCD was formulated and manufactured to contain 41% carbohydrates (Table 1). The experimental diet was supplemented with a premix of crystalline L-amino acids according to the amino acid profile of the dorsal muscles of zebrafish, including Ala, Arg, Asp, Gly, and Lys (25).

Growth experiment. All male zebrafish were maintained at 28.5°C with a photoperiod cycle of 14 h of light and 10 h of darkness (59). The growth trial was conducted in 120-liter aquariums with a recirculating system (1 l/min) and biology/mechanical filtration. The three genetic groups of zebrafish were initially raised with *Artemia salina* until 60 dpf. Twenty male fish of each genotype were then randomly selected and stocked in one aquarium at a mean weight of 0.193 ± 0.002 g. Three replicate aquariums were used in this study. During the 60-day experiment, fish were fed with a HCD to apparent satiation three times per day at 0830, 1230, and 1630. We identified the genotype of each fish at the end of the growth trial. Final fish weight from each genotype group and survival rate in each aquarium were then determined. We repeated the entire growth trial with the same conditions described in this section to measure food intake, oxygen consumption, and anabolic rate of the fish from the three genotype groups.

Food intake measurement. After the growth trial, 18 fish of each genotype were randomly selected and separately allocated into three aquariums. All fish from nine aquariums (3 aquariums for 1 genotype) were then acclimated for 1 wk under the same conditions as the above growth experiment. Before the food intake was measured, fish were starved for 24 h and weighed. Then, fish were fed to apparent satiation three times a day for 1 wk, and daily food intake was recorded. Relative food intake (feeding rate) was calculated as follows: feeding rate (%/day) = 100 × (food intake/initial body weight)/days.

Oxygen consumption. After the growth trial, oxygen consumption of the fish from the three genotype groups was measured as described previously (34). Briefly, fish were starved for 48 h, weighed, transferred, and maintained individually in separate respiration chambers ($n = 6$ for 1 genotype) with 1 liter of fresh water at 28°C. Oxygen concentration was measured using a SevenGo pro-SG6 oximeter (Analytical, CH-8603; Mettler-Toledo; Columbus, OH) after 6 h of enclosure within the chamber. The oxygen concentration in the respiration chamber without any fish during the same period was treated as the initial oxygen concentration. Oxygen consumption was expressed as milligrams per O_2 per hour per gram of body weight.

In vivo anabolic rate assay. After the growth trial, 10 fish of each genotype were used to perform the anabolic rate assay. The anabolic assays of intraperitoneally injected L-[^{14}C(U)] amino acid mixture

(received an injection of 0.025 μCi/4 μl DMSO per gram of body weight) or palmitic acid [1-^{14}C] (received an injection of 0.02 μCi/4 μl DMSO per gram of body weight) were performed in live fish as previously described (42). Two houre after injection with L-[^{14}C (U)] amino or [1-^{14}C] palmitic acid, tissues (liver, muscle) and whole body from each genotype group were sampled. In addition, 2 h after the injection with [1-^{14}C] palmitic acid, total lipids from each fish genotype were extracted and weighed. Tissues, whole body and total lipids from each fish genotype were then digested with $HClO_4/H_2O_2$ (2:1) at 60°C. The retention of radioactivity from different tissues, whole body, or total lipids was determined using a Tri-Carb 4910TR Liquid Scintillation Analyzer (PerkinElmer, Waltham, MA).

Sampling. At the end of the growth trial, eight fish of each genotype in each aquarium were randomly sampled 1 h after feeding. Fish were anesthetized in 0.02% ice-cold MS-222 (cat. no. A5040; Sigma, St. Louis, MO). The caudal fin was severed with scissors, and whole blood was collected from the wound with heparin-treated tips. Blood samples from three fish of each genotype in each aquarium were used for blood glucose measurement. Plasma was then isolated from the blood of remaining five fish by centrifugation at 4°C (1,500 *g* for 15 min) and stored at −80°C for later analysis. After blood sampling, liver, muscle, and pituitary tissues were immediately sampled for mRNA and protein analysis and visceral mass was sampled for lipid extraction.

Nile Red staining and Oil Red O staining. Neutral lipid accumulation was visualized using fluorescent dye staining in live fish. One fish of each genotype in each aquarium (3 fish per genotype) was sampled for Nile Red staining. Nile Red (N3013; Sigma) was dissolved to a concentration of 0.1 μg/ml. Both mutant and control fish were immersed at 28°C overnight in the dark. Images were obtained using an Olympus SZX16 FL stereomicroscope (Olympus, Tokyo, Japan) at an excitation wavelength of 488 nm. The liver of one fish of each genotype in each aquarium (3 fish per genotype) was initially fixed in 4% paraformaldehyde and then sectioned with a cryostat. Frozen sections were stained with Oil Red O to visualize fatty droplet accumulation in the liver.

Biochemical analyses. Blood glucose levels were measured using a blood glucose monitor (Accu-Chek Performa; Roche, Basel, Switzerland). Plasma and liver triglycerides (TGs) were measured using a Triglyceride Colorimetric Assay Kit (Cayman Chemical, Ann Arbor, MI) according to the manufacturer's instructions. Plasma cholesterol, nonesterified fatty acids (NEFAs), and phospholipids were measured using LabAssay cholesterol, NEFA, and phospholipid kits (Wako Pure Chemical Industries, Tokyo, Japan), respectively.

Proximate compositions were determined according to the methods described by the Association Official Analytical Chemists (18). Eight zebrafish of each genotype per aquarium were randomly selected, frozen in liquid nitrogen for 3 h, and stored at −80°C for 24 h. The eight fish were then mixed as one sample and ground into a powder after they were freeze dried (Alpha 1–4 LD plus; Martin Christ, Osterode, Germany) for 24 h. Crude protein content (N × 6.25) was determined by the Kjeldahl method after acid digestion using a 2300 Kjeltec Analyzer Unit (FOSS Tecator, Haganas, Sweden). Crude lipid content was determined by ether extraction in a Soxtec system (Soxtec System HT6; Tecator). Crude ash content was determined by incineration in a muffle furnace at 550°C for 12 h. Moisture content was determined by oven drying at 105°C until samples reached a constant weight. Visceral mass lipid content was determined following homogenization in chloroform/methanol (2:1, vol/vol) according to the method described by Folch et al. (12).

Quantitative real-time PCR. Total RNA was extracted from liver and adipose tissue samples using TRIzol reagent and cDNA was synthesized using an oligo (dT) 18 primer and the Revert Aid First-Strand cDNA Synthesis Kit (K1622; Thermo Scientific, Waltham, MA) according to manufacturer's instructions. Quantitative (q)PCR primers were designed using the National Center for Biotechnology Information primer BLAST service and are listed in Table 2. All mRNA levels were calculated as fold expression relative to the housekeeping gene, *GAPDH*. All samples were run in triplicate, and the results are expressed according to the method described by Bustin et al. (4).

Western blot analysis. Total hepatic, pituitary and muscle proteins were extracted using a protein extraction buffer (Thermo Scientific) according to the manufacturer's instructions. Equal amounts of protein were subjected to SDS-PAGE and transferred to PVDF membranes. The PVDF membranes were blocked with 5% milk in TBS Tween and then incubated with anti-GCK (HPA007093; Sigma), anti-AKT [9272S; Cell Signaling Technology (CST), Danvers, MA], anti-AMPKα (2532S; CST), anti-insulin grwoth factor-1 (anti-IGF-1; ab9572; Abcam, Cambridge, UK), anti-phospho-AKT^{s473} (4060S; CST), anti-phospho-AMPKα^{Thr172} (2535S; CST), anti-phospho-S6$^{ser240/244}$ (2215S; CST), anti-phospho-STAT5A/B$^{Tyr694/699}$ (2189940; Millipore, Billerica, MA), anti-phospho-PPARα^{s12} (ab3484; Abcam), anti-GH1 (a gift from Dr. Wei Hu, Institute of Hydrobiology, Chinese Academy of Sciences), and anti-GAPDH (ab70699; Abcam) antibodies. The antibodies were used at a 1:1,000 dilution. Horseradish peroxidase-labeled secondary antibodies were used to generate a chemiluminescent signal that was detected with a CCD camera-based imager (Chemidoc MP Imaging System; Bio-Rad). GAPDH served as a control. All samples were repeated three times.

Statistical analysis. Data were analyzed with GraphPad Prism 5.0. All results are presented as means ± SE. Differences were assessed using a one-way ANOVA. For all statistical comparisons, $P < 0.05$ was used to indicate a statistically significant difference.

RESULTS

Blood glucose and glucose metabolism. Compared with control siblings, *insra*−/− fish and *insrb*−/− fish showed higher blood glucose levels than control fish at 1 h postprandial (Fig. 1*A*). This outcome was consistent with the measurement of total glucose in *insra*−/−, *insrb*−/−, and control fish at the larval stage (60). It was worth noting that the glucose level in *insra*−/− fish was higher than that in *insrb*−/− fish, which suggested a more critical role of Insra than Insrb in glucose metabolism. As observed in the Western blot analysis, the amount of GCK protein, involved in glycolysis (43), was significantly decreased in *insra*−/− fish and *insrb*−/− fish compared with the control fish, with *insra*−/− fish showing the greatest decrease in protein levels (Fig. 1, *B* and *C*).

We subsequently explored the expression of genes involved in glycolysis using real-time qPCR. These genes included *hexokinase domain containing 1* (*hkdc1*), *glucokinase* (*gck*); *aldolase a* (*aldoaa*); *pyruvate kinase, liver, and RBC* (*pklr*); and glucose-6-phosphate isomerase a (*gpia*) (Fig. 1*D*). The results demonstrated that the transcripts involved in glycolysis, *hkdc1*, *gck*, *aldoaa*, *pklr*, and *gpia* were decreased in both *insra*−/− and *insrb*−/− fish, which suggested that glycolysis was downregulated when the *insr* was depleted. These results indicated that both *insra* and *insrb* played pivotal roles in glycolysis and they partially explained why *insra*−/− fish showed higher levels of blood glucose than *insrb*−/− fish or control fish. The *glucose-6-phosphatase a, catalytic subunit, tandem duplicate 1* (*g6pca.1*) gene, involved in gluconeogenesis, was significantly downregulated in both *insra*−/− and *insrb*−/− fish (Fig. 1*D*).

A previous study indicated that the insulin-signaling pathway regulated glucose homeostasis through the downstream AKT-signaling cascade (6, 24, 62). Thus we examined the levels of total AKT (T-AKT) and phosphorylated AKT (P-AKT) protein. As expected, P-AKT levels in *insra*−/− fish

Table 2. *Primer sequences used for quantitative real-time PCR*

Gene	Accession No.	Forward Primer (5′–3′)	Reverse Primer (5′–3′)	Product Size (bp)
Insulin signaling pathway-related genes				
pik3cd	NM_201199.1	CTGTCTGGCATCTGTCCTGC	TTCAGTGCATCGTGTCGCAA	186
pik3ca	XM_009306177.2	CGTTCATGCACTGTTCGCTA	TGGGACAGCCATATGGTACAC	243
ppp1caa	NM_214811.2	CCCTGTTCTCCGCTCCTAAC	GAGGGTGGTGGGAGTCCAT	232
ppp1r3da	NM_001110412.2	CTGCACAGAGTTTGTGTCGC	CCCACCAGGAGAATCCGATG	112
pde3b	XM_686791.8	GTGAGAGGACCCTTTGGTGG	TGGCACCATTATCCCGTCTG	116
prkag2a	NM_001077179.2	ACTTCCACCTCCGTGATTCG	GACAGAGTGGAGCTCAGACG	178
irs2a	NM_200315.1	GCTCAGATGGAAAAGCTGCG	TTGGCCTCTTCGGCTTGATT	226
mknk2b	NM_194402.1	CGGGGTTTCCCGTTAAAAGC	TTATTTGGACTGGCGGCAAC	104
shc2	NM_001044973.1	GACCAGGGTGGAGGGAATA	GAGATGTTGACGCCGATG	342
socs2	NM_001114550.1	AAGGCAGGACTAACCAAATCG	TTGATGGCAATACGGCACAGG	112
socs1a	NM_001003467.1	GCCTGCTCTTGGAGTACTTG	CCTGGATCTTTGGGATTGGAA	205
Glycolysis-related genes				
hkdc1	NM_001115125.1	CATCCTTTCAGAGGACGGCA	CCAAGAACCACCGCTTCAAC	223
gck	NM_001045385.2	CACCGCTGACCTGCTATGAT	AGTCGGCCACTTCACATACG	102
aldoaa	NM_194377.2	AGGCTGATCCGTGAGTGTTG	GCCACGCTACCTGTAGACTC	188
pklr	NM_201289.1	TCCTGGAGCATCTGTGTCTG	GTCTGGCGATGTTCATTCCT	144
gpia	NM_144763.1	ACTGTACGGTCGTGTTTCCC	ATGTTGAGGTTTCCCACGCT	131
Gluconeogenesis-related gene				
g6pca.1	NM_001003512.2	GCTGCACCATACGAGATGGA	TCACCAAACAGCACCCACTT	248
Protein synthesis-related genes				
igf1	NM_131825.2	TCGTCCCCACTCTTGTAAAGC	TGGCGATGGAGCTTGAACAT	116
igf1rb	NM_152969.1	GCCTCAGAGCTGGAGAACTTC	CGTTGTTGCGGAAATCTCTTTC	331
ulk2	XM_002664615.4	AGAACACAAGCCGAAGGGAT	ATTCCTCCTAACCGCGTGAC	249
mat2aa	NM_001290080.1	CTTCCCGTGAAATGTAGGCAG	TAAAAACAACATGGCCTGCGG	184
stat1b	NM_200091.2	ACGTCCACGTTGAAAGGTAA	AGCTGCTTTACGTGGCATTTC	104
bcat1	NM_200064.1	AGGAGACTGCAAGATGGGAGG	TGCCGACTGGACTGACAACAC	371
4ebp1	NM_199645.1	GTTGTGCCTGAAAGAGCCAC	AAACAAAGTGTGGCATGGCG	116
Lipolysis-related genes				
acsl1b	NM_001003569.2	CTGACGAGTTCGGTCGAGTT	TGGCGTACCAGTATGCAGTG	177
cpt1b	NM_001328192.1	TGAGACGGATTCTTTCCGCT	TTCGCTAGGCTTGTTACTTGC	242
cpt2	NM_001007447.1	AATGGATTGGGTGCAACGTG	TGAGTTCTAACCTTCAGGCTCT	240
lipca	NM_201022.1	GGACCGCAGCTTACTTTTGG	TCCGACTGGATGTGAAAGTGT	191
fabp1a	NM_001044712.1	TCGTTCTGCTTGAACATGCG	GCTGTCTCACCATGAAGCAAC	162
Lipogenesis-related genes				
fas	DQ812117.1	TCCAAGAGTTCAAACACGGT	TGAGTGACACCACAACAG	196
foxo1a	NM_001077257.2	AGCCTGTCTGAAATGGCTGG	TGCTGGCTTACTGCCGATAG	212
fads2	NM_131645.2	CCAATCAGAGCGAGCCTTCA	ACGCATTCAAAGTGCCACAA	136
elovl5	NM_200453.2	TTTCGGCTAGAAGGAAAGCAGT	GAACCGAAAGTGGGAGGTG	201
acc	NM_001271308.1	ATGGCAGAGCAAGACTCCAC	CCTCTGCAGGTCGATACGTC	294
pparγ	DQ017619	AGCGACAATGCTCCTTTT	CACTTCGATGACCCCGTA	270
Reference gene				
gapdh	NM_001115114.1	GTCCACTGACTTCAATGGGGA	CCAGATGGGAGAATGGTCGC	217

and *insrb*−/− fish were lower compared with control fish. It is worth noting that P-AKT levels were higher in *insra*−/− fish compared with *insrb*−/− fish (Fig. 1, *E* and *F*), which was likely due to the increased expression of insulin-like growth factor 1 (*igf1*) and insulin-like growth factor 1 receptor (*igf1r*) in *insra*−/− fish (see below). This may also activate the AKT-signaling pathway (57, 63).

Body weight, food intake, and oxygen consumption. To investigate the individual physiological function of *insra* and insrab in insulin-signaling pathways, an HCD was provided to amplify the redundant and overlapping roles of each receptor in fueling homeostasis. After 60 days of being fed with *Artemia salina*, growth performance and biochemical analysis were conducted (Table 3). Out of *insra*−/−, *insrb*−/−, and control fish, only *insrb*−/− fish demonstrated decreased protein but increased lipid content. However, the divergence of body composition could not be observed visually. After the 60-day HCD growth trial, the body weight of control and knockout fish markedly diverged, with both *insra*−/− fish and *insrb*−/− fish demonstrating significant increases in body weight compared with control fish (Table 4). The increased body weight gain in *insra*−/− fish and *insrb*−/− fish compared with control fish led us to further measure food intake of the fish from the three genotype groups. As expected, *insra*−/− fish and *insrb*−/− fish had significantly higher feeding rates than control fish (Fig. 2*A*). To assess energy expenditure, we tested oxygen consumption rate and found that there was no significant difference in oxygen consumption between mutants and control fish (Fig. 2*B*).

AMPK signaling has a close relationship with the metabolism and energy requirements of organisms. To explore anabolic levels, we examined AMPK protein. A significant decrease in phosphorylated AMPK (P-AMPK) was observed in *insra*−/− or *insrb*−/− fish (Fig. 2, *C* and *D*). As it is a cellular energy sensor responding to low ATP levels (38), decreased P-AMPK seen here suggests that catabolic pathways, such as the biolysis of lipids and proteins that generate ATP, may be switched off (35). The increased body weight in *insra*−/− or *insrb*−/− fish may be tightly linked to AMPK-signaling inhibition.

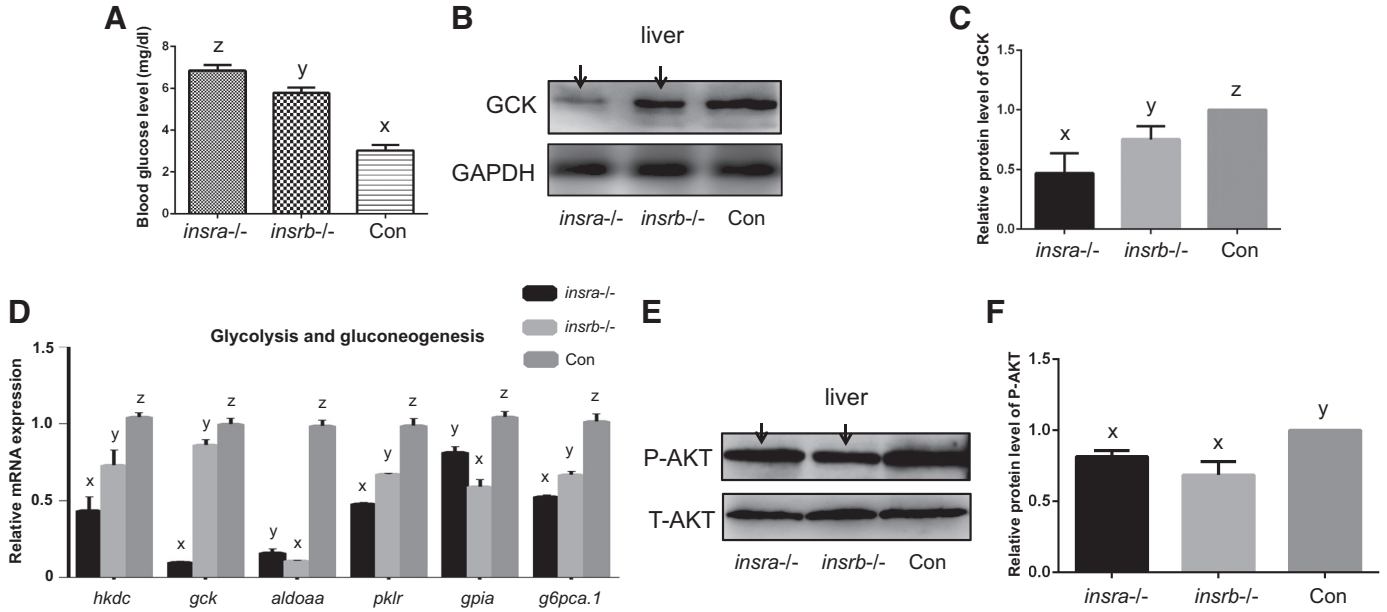

Fig. 1. Analyses of glucose metabolism in *insra*−/− or *insrb*−/− fish. *A*: blood glucose levels in *insra*−/− fish, *insrb*−/− fish, and control fish ($n = 5$ for each genotype). *B*: GCK protein levels in liver samples of *insra*−/− fish, *insrb*−/− fish, and control fish ($n = 3$ for each genotype per time). *C*: quantification of relative GCK protein levels from the Western blot are shown in *B*. *D*: the expression levels of *hkdc1*, *gck*, *aldoaa*, *pklr*, *gpia*, and *g6pca.1* in liver samples of *insra*−/− fish and *insrb*−/− fish were significantly affected compared with control fish ($n = 3$ for each genotype per time). *E*: phosphorylated (P)-AKT and total (T)-AKT protein levels in liver samples of *insra*−/−, *insrb*−/−, and control fish ($n = 3$ for each genotype per time). *F*: quantification of relative protein levels of P-AKT from the Western blot are shown in *E*. The letters *x*, *y*, and *z* in the bar chart represent significant differences of each index in *insra*−/− fish, *insrb*−/− fish, and control fish ($P < 0.05$). The green arrows indicate downregulated levels of the nominated proteins. All protein and mRNA measurements were repeated 3 times independently.

HCD results in lipid accumulation to hepatic steatosis in insrb−/− fish. After the analysis of growth performance, we carried out body composition analysis. We observed that crude protein content in the *insrb*−/− group was decreased compared with the *insra*−/− and control fish, whereas crude lipid, carcass lipid, and visceral mass lipid content were significantly higher in the *insrb*−/− group compared with the *insra*−/− and control fish (Table 4).

Since abdominal adiposity accumulation in *insrb*−/− zebrafish was more significant compared with *insra*−/− and control fish, analysis of neutral lipids with Nile Red staining was carried out in the three groups. As expected, the Nile Red fluorescence significantly increased in visceral adipose tissue in *insrb*−/− fish compared with *insra*−/− and control fish after 60 days of HCD feeding (Fig. 3, *A–C*). These results were similar to the body composition results, i.e., the highest content of crude lipid, especially visceral mass lipid in *insrb*−/− fish.

Table 3. *The initial whole body proximate composition of insra−/−, insrb−/−, and control zebrafish before the feeding trial*

	Genotype		
Whole body composition	*insra*−/−	*insrb*−/−	Control
Moisture, %	70.23 ± 0.00^{y}	67.47 ± 0.01^{x}	69.43 ± 0.00^{y}
Crude protein, %DM	47.52 ± 0.16^{y}	45.63 ± 0.62^{x}	51.80 ± 0.10^{y}
Crude lipid, %DM	32.55 ± 0.08^{y}	37.24 ± 0.75^{z}	30.88 ± 0.09^{x}
Ash, %DM	8.34	9.04	8.49

Values are means ± SE of 3 replicate groups ($n = 3$). Labeled means in a row without a common letter are different, $P < 0.05$. Values for whole composition were obtained from composite samples per replicate group ($n = 3$). For ash, 3 fish from each genotype were mixed as one sample. DM, dry matter. $^{x,y,z}P < 0.05$, significant differences of each index in *insra*−/− fish., *insrb*−/− fish, and control fish.

Adipocytes activate lipolysis and the breakdown of TGs into free fatty acids, which are transferred into liver mitochondria to undergo β-oxidation for generating ATP for the organisms (44). Since the liver is a central organ that is implicated in lipid metabolism and homeostasis, the pathological features of the liver were examined with Oil Red O staining. Increased lipid accumulation and hepatic steatosis were observed in the liver in *insrb*−/− fish compared with *insra*−/− and control fish (Fig. 3, *D–F*). We also quantified fat droplets in the liver and observed that, although the number of fat droplets were decreased in *insrb*−/− fish livers, the average area and frequency distribution of fat droplets significantly increased compared with the control fish (Fig. 3, *G–I*). We also examined adipose tissue morphology in visceral organs and found that the distribution of adiposity significantly increased in *insrb*−/− fish (Fig. 3, *J–L*). All these results suggest that depletion of *insrb* leads to accumulated adiposity and compromised hepatic steatosis. In all, *insra* or *insrb* knockout fish exhibited different effects on lipid and protein metabolism.

We subsequently performed biochemical measurements to examine the quantities of plasma and liver TG, plasma NEFA, plasma cholesterol, and plasma phospholipid in the three groups. Plasma and hepatic TG levels in the *insrb*−/− groups were significantly higher compared with the other two groups (Fig. 4, *A* and *B*). Meanwhile, in the plasma of *insrb*−/− fish, NEFA, cholesterol, and phospholipids were also increased compared with *insra*−/− fish and control fish (Fig. 4, *C–E*). It was also worth noting that these indices were significantly decreased in *insra*−/− fish compared with control fish. Taken

Table 4. *Growth performance, body condition indexes and whole body proximate composition of insra−/−, insrb−/−, and control zebrafish fed with the high-carbohydrate diet for 8 wk*

Variables	Genotype		
	insra−/−	*insrb−/−*	Control
Initial body weight, g	0.195 ± 0.00	0.191 ± 0.00	0.195 ± 0.00
Final body weight, g	0.365 ± 0.01^{y}	0.343 ± 0.01^{y}	0.311 ± 0.00^{x}
Relative weight gain, %	83.94 ± 3.14^{y}	80.27 ± 6.52^{y}	59.50 ± 1.44^{x}
Initial body length, mm	28.67 ± 0.56	28.5 ± 0.34	29.17 ± 0.31
Final body length, mm	33.06 ± 0.36	32.67 ± 0.27	32.44 ± 0.25
Survival, %	98.33 ± 1.67	96.67 ± 1.67	98.33 ± 1.67
Condition factor, g/cm^3	1.45 ± 0.03^{xy}	1.48 ± 0.05^{y}	1.33 ± 0.01^{x}
Whole body composition			
Moisture, %	69.23 ± 0.00^{y}	66.47 ± 0.00^{x}	68.43 ± 0.00^{y}
Crude protein, %DM	50.79 ± 0.66^{y}	46.68 ± 1.25^{x}	49.18 ± 0.85^{xy}
Carcass protein content, %DM	52.54 ± 0.26^{xy}	51.41 ± 0.39^{x}	53.33 ± 0.23^{y}
Crude lipid, %DM	26.66 ± 0.39^{x}	36.52 ± 0.55^{z}	29.16 ± 0.32^{y}
Carcass lipid content, %DM	25.31 ± 0.42^{x}	26.66 ± 0.16^{y}	24.95 ± 0.26^{x}
Visceral mass lipid, %DM	55.33 ± 0.04^{x}	63.28 ± 0.06^{x}	58.05 ± 0.03^{y}
Ash, %DM	9.88	10.44	9.99

Values of means of 3 replicate groups (n = 3). Labeled means in a row without a common letter are different, $P < 0.05$. Condition factors (g/cm^3) = (body weight × 100)/(body length^3). Values for whole body composition were obtained from composite samples per replicate group (n = 3). For ash, 3 fish from each genotype were mixed as 1 sample. DM, dry matter. $^{x,y,z}P < 0.05$, significant differences of each index in *insra−/−* fish, *insrb−/−* fish, and control fish.

together, our results suggested that lipid synthesis in *insra−/−* fish and lipid utilization in *insrb−/−* fish were affected compared with the control fish.

Insrb is involved in protein synthesis via regulating growth hormone sensitivity. Since *insrb−/−* fish exhibited accumulated visceral adipocyte and total lipid content, but decreased protein content, we hypothesized that the pathway that promotes lipid utilization and protein synthesis may be impaired with depletion of *insrb*. We examined the growth hormone (GH)-signaling pathway, in which mitochondrial fatty acid β-oxidation and protein synthesis were promoted (26, 33, 39). In contrast to control fish, *insrb−/−* fish showed diminished phosphorylation levels of Stat5 (P-STAT5) in muscle (Fig. 5, *A–C*), which suggested that lipid accumulation may be result from a compromised GH-signaling pathway (7, 27, 29). Additionally, previous studies have indicated that protein synthesis induced by growth hormone requires signaling through mammalian target of rapamycin and GH treatment can enhance the phosphorylation of ribosomal protein S6 (P-S6) (15). Thus we subsequently examined the levels of P-S6 in muscles, where GH exerted direct effects. P-S6 was also diminished in *insrb−/−* fish (Fig. 5, *A–C*). IGF-1 is a prominent mediator of the effects of GH on skeletal growth (9, 34). IGF-1 was also decreased in the *insrb−/−* fish liver (Fig. 5, *D–F*). For lipid utilization, we examined the levels of P-PPARα in the liver. Again, *insrb−/−* fish showed diminished P-PPARα in the liver (Fig. 5, *D–F*). Combined with a previous study showing that the insulin increased PPARα phosphorylation and enhanced transcriptional activity of PPARα (47), we proposed that insulin promoted phosphorylation of PPARα via Insrb. The amount of pituitary GH protein dramatically increased, which indicated that, although the mechanism was unknown, *insrb* deficiency led to GH resistance (Fig. 5, *G* and *H*). All these results suggested that the effects of GH on protein synthesis and lipolysis were impaired in the absence of Insrb.

We then assessed transcriptional levels of some key elements involved in the insulin-signaling pathway in the liver to investigate the effects of each insulin receptor on the insulin-signaling pathway (Fig. 6*A*). With the exception of *shc2*, *socs1a*, and *socs2*, we found that most of the insulin-signaling pathway genes were significantly downregulated in *insrb−/−* fish compared with control fish. Downregulated genes included *phosphatidylinositol-4,5-bisphosphate 3-kinase catalytic subunit delta* (*pik3cd*); *phosphatidylinositol-4,5-bisphosphate 3-kinase catalytic subunit alpha* (*pik3ca*); *protein phosphatase 1 catalytic subunit alpha isozyme a* (*ppp1caa*); *phosphodiesterase 3B* (*ped3b*); *protein kinase, AMP-activated, gamma 2*

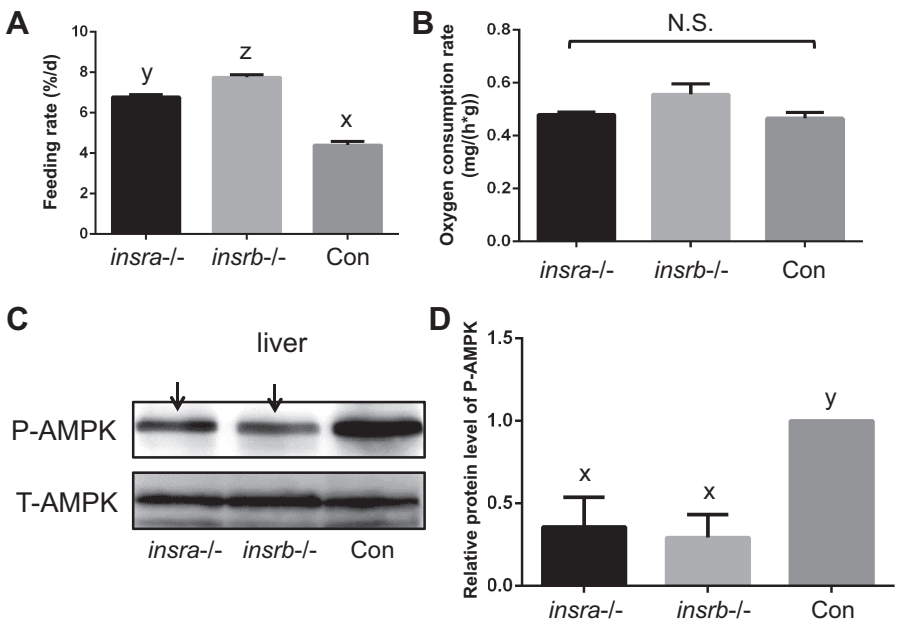

Fig. 2. Measurements of feeding rate and oxygen consumption. *A*: measurement of food intake rate in zebrafish of 3 genotypes (n = 18 for each genotype, divided into 3 groups). *B*: measurement of oxygen consumption rate in zebrafish of 3 genotypes (n = 18 for each genotype, divided into 3 groups). *C*: phosphorylated (P)-AMPK and total (T)-AMPK levels in liver samples of *insra−/−*, *insrb−/−*, and control fish (n = 3 for each genotype per time). *D*: quantification of P-AMPK relative protein levels from the Western blot are shown in *C*. The letters *x*, *y*, and *z* in the bar chart represent significant differences of each index in *insra−/−* fish, *insrb−/−* fish and control fish ($P < 0.05$). N.S., no significance. The green arrows indicate downregulated levels of the nominated proteins. All protein measurements were repeated 3 times independently.

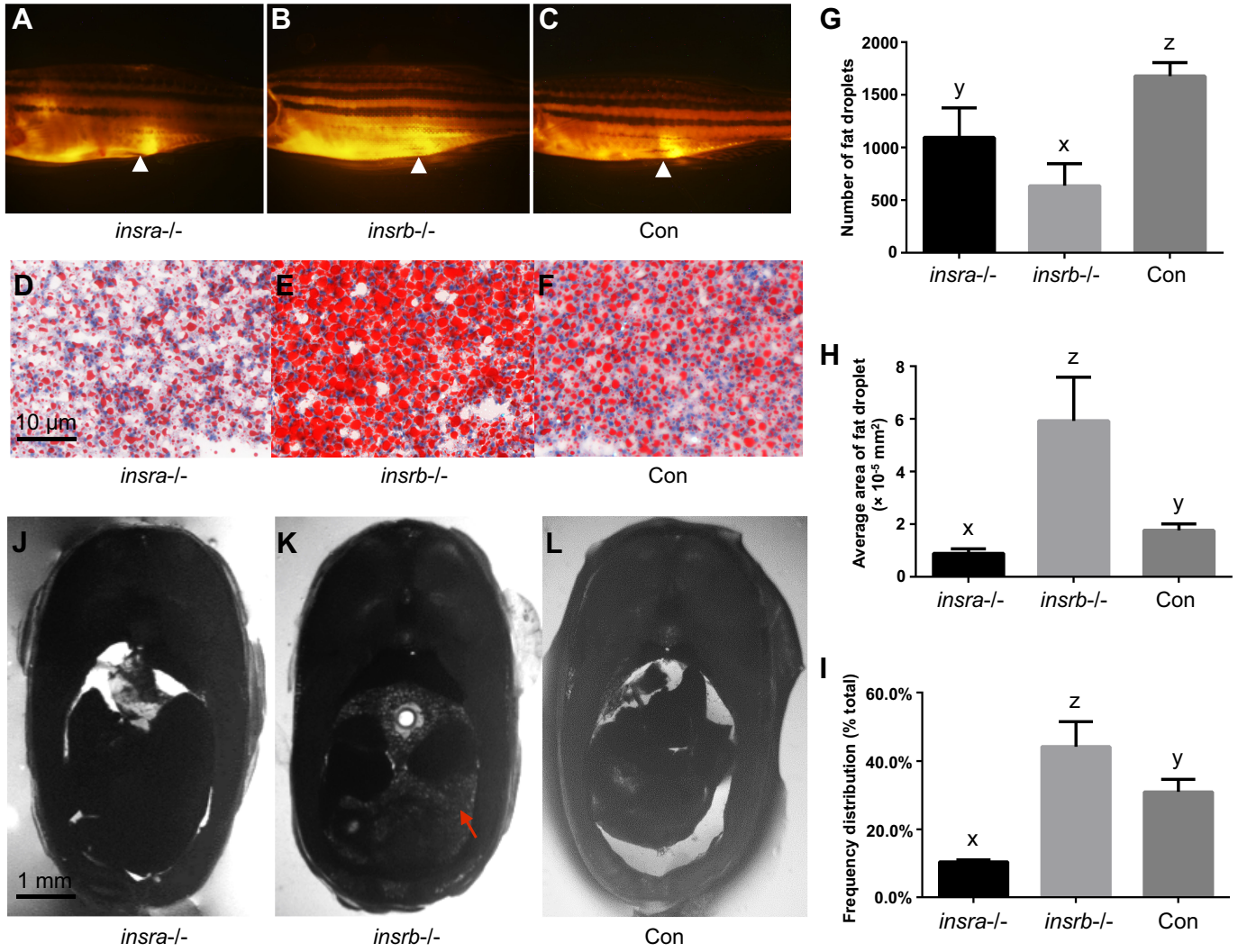

Fig. 3. Observations of neutral adipose tissues and liver fatty droplets. *A–C*: Nile Red fluorescence staining of adult zebrafish ($n = 3$ for each genotype). Lateral view anterior is to the *left*. White arrowheads: visceral adipose tissue. *D–F*: Oil Red O staining of adult zebrafish liver sections ($n = 3$ for each genotype) for *insra*−/− fish (*D*), *insrb*−/− fish (*E*), and control fish (*F*). *G–I*: quantification of the fat droplets number, the average area of fat droplets, and the frequency distribution of fat droplets in 3 samples of each genotype. The statistical analysis of the number, average area, and frequency distribution of fat droplets in *G–I* is calculated per analyzed area. *J–L*: cross sections through trunks of adult mutants and their controls show excessive visceral adipose tissue in the *insrb*−/− fish ($n = 3$ for each genotype). The letters *x*, *y*, and *z* in the bar chart represent significant differences of each index in *insra*−/− fish, *insrb*−/− fish, and control fish ($P < 0.05$). Red arrow indicates visceral adipose tissue.

noncatalytic subunit a (*prkag2a*); *inulin receptor substrate 2a* (*irs2a*); *MAP kinase interacting serine/threonine kinase 2b* (*mknk2b*); and *protein phosphatase 1 regulatory subunit 3Da* (*ppp1r3da*). However, compared with control fish, *insra*−/− fish exhibited a slight influence on the insulin-signaling pathway. Compared with the control fish, there was a significant increase in expression of the suppressor of GH signaling, *shc2*, *socs1a*, and *socs2* (7), indicating that IGF-1/IGF-1 receptor signaling was overactivated when *insra* was depleted.

Furthermore, the relative gene expression levels of *igf1* and its receptor, *igf1r*, were significantly higher in *insra*−/− fish than the other two groups. Genes involved in protein synthesis, such as *unc-51-like autophagy activating kinase 2* (*ulk2*), *methionine adenosyl-transferase II alpha a* (*mat2aa*), *signal transducer and activator of transcription 1b* (*stat1b*), *branched chain amino-acid transaminase 1, cytosolic* (*bcat1*), and *eukaryotic translation initiation factor 4E-binding protein* (*4ebp*) were also increased in the absence of Insra (Fig. 6*B*). These observations indicate that protein synthesis is activated via the insulin/insrb pathway under HCD. All these results suggest that Insrb is involved in lipid utilization and protein synthesis by mediating the sensitivity of the GH-signaling pathway.

Changes in mRNA levels of enzymes involved in lipolysis, mobilization and fatty acid β-oxidation, such as cyl-CoA synthetase long-chain family member 1b (*acsl1b*), carnitine palmitoyltransferase 1B (*cpt1b*), *carnitine palmitoyltransferase 2* (*cpt2*), lipase alpha (*lipca*), and fatty acid binding protein (*fabp*) were significantly increased in *insrb*−/− fish liver (Fig. 6*C*). These may be compensatory effects due to dual effects of failure of PPARα activation and GH-signaling pathway deficiency.

Insra is involved in lipid synthesis. During the biochemical measurements, we also observed that *insra*−/− fish had the lowest levels of plasma and hepatic TG, plasma NEFA, and

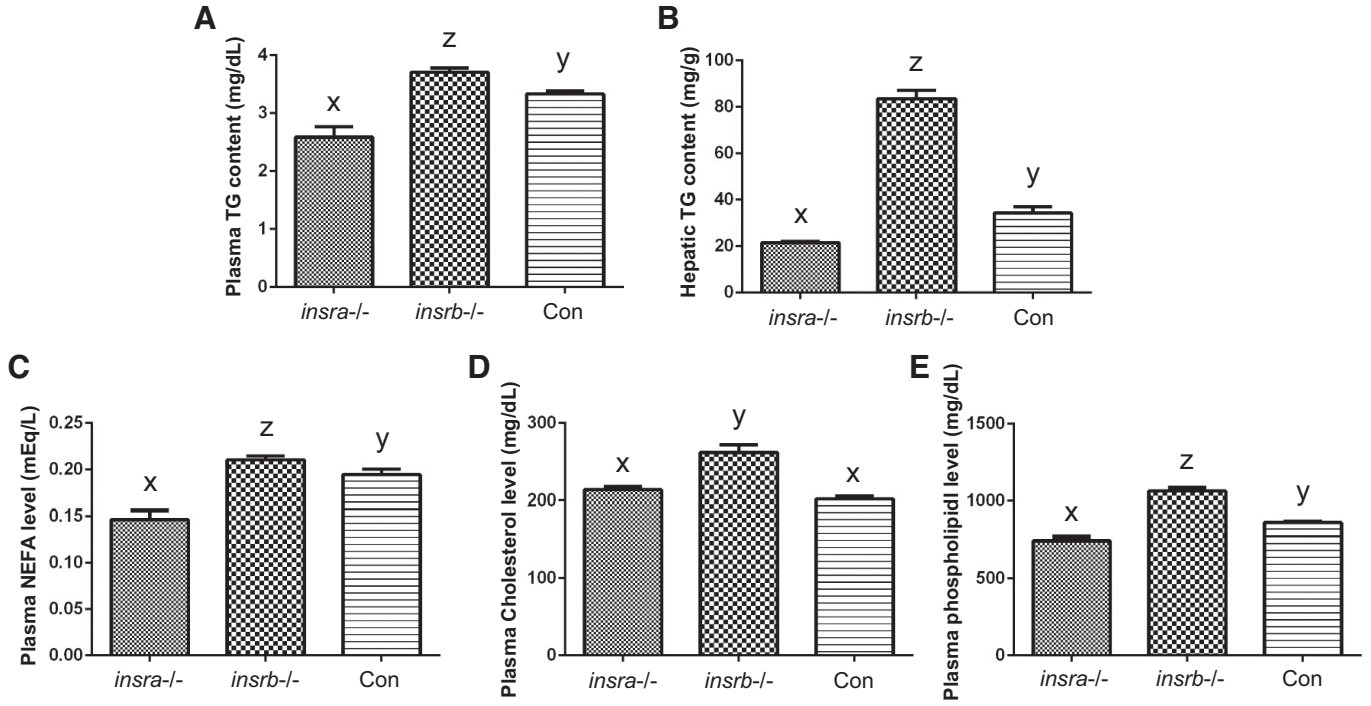

Fig. 4. Measurement of triglyceride (TG), nonesterified fatty acid (NEFA), cholesterol, and phospholipid. *A*: bar charts represent the quantification and statistical analyses of plasma TG levels. *B*: bar charts represent the quantification and statistical analyses of hepatic TG levels. *C*: bar charts represent the quantification and statistical analyses of plasma NEFA levels. *D*: bar charts represent the quantification and statistical analyses of plasma cholesterol levels. *E*: bar charts represent the quantification and statistical analyses of plasma phospholipid levels. The letters *x*, *y*, and *z* in the bar chart represent significant differences of each index in *insra*−/− fish, *insrb*−/− fish, and control fish ($P < 0.05$); $n = 3$ for each genotype.

plasma phospholipids (Fig. 4, *A–C*, and *E*). Together with increased blood glucose levels and decreased visceral and whole body lipid content in *insra*−/− fish compared with control fish, we hypothesized that Insra may be responsible for lipid synthesis from glucose. Consistent with the relative expression levels of the genes involved in protein synthesis in *insra*−/− fish, we also observed increased levels of proteins involved in protein synthesis in muscle, P-S6 and P-STAT5, as well as increased IGF-1 and P-PPARα in the liver in *insra*−/− fish (Fig. 5, *A* and *B*). This outcome explains the composition measurement results in *insra*−/− fish (Table 4), i.e., increased protein gain and decreased lipid content. These results suggested that, when *insra* was depleted, the transition from glucose to lipid was compromised, while protein synthesis was activated and growth was facilitated via the insulin/insrb pathway under HCD.

Expression of lipogenesis enzymes, *fatty acid synthase* (*fas), fatty acid desaturase 2* (*fads2*), *fatty acid elongase 5* (*elovl5*), *acetyl-CoA carboxylase alpha* (*acc*), and *forkhead box protein O1* (*foxo1a*) was assayed by real-time qPCR. Uniformly, *fas*, *fads2*, *elovl5*, and *acc* all showed the greatest decrease in *insra*−/− fish (Fig. 6*C*). Downregulated expression of genes involved in lipogenesis was observed in *insra*−/− fish, which suggests that impaired lipid synthesis occurs by failure to activate the expression of key enzymes involved in lipogenesis. However, the downregulation of these genes involved in lipogenesis was not observed in *insrb*−/− fish, except for the key molecule that inhibits lipogenesis but promotes lipolysis, *foxo1a* (41). To better elucidate the role of Insra in lipid synthesis, the expression of *fas* and *pparγ*, which are essential in lipid synthesis (30), was quantified in adipose tissue. Significantly, *fas* and *pparγ* expression were significantly diminished in *insra*−/− fish (Fig. 6*D*). Combined with the failure of glucose utilization in *insra*−/− fish, we conclude that Insra is implicated in lipid synthesis from glucose, while the accumulation of lipids in *insrb*−/− fish may be due to failure of lipid catabolism, which is reflected through the downregulation of P-PPARα and *foxo1a* and GH-signaling pathway deficiency in the liver of *insrb*−/− fish.

Protein and lipid synthesis. To further confirm the role of Insra or Insrb in the regulation of protein synthesis or lipid synthesis directly, we performed an anabolic assay in vivo by testing the retention of radioactivity 2 h after intraperitoneal injection with L-[^{14}C(U)] amino acid mixture or palmitic acid [1-^{14}C]. The retention of the amino acid mixture in *insra*−/− fish was slightly high in muscle and in the whole body ($P > 0.05$) compared with control fish (Fig. 7, *A–C*). The retention of fatty acids in muscle and liver and the whole body and total lipid of *insrb*−/− fish were significantly higher ($P < 0.05$) than the other two groups (Fig. 7, *D–G*). These results directly indicated that lipid synthesis is promoted when *insrb* is depleted.

DISCUSSION

In the present study, we observed an interesting phenotype where weight gain in *insra* or *insrb* knockout zebrafish markedly increased compared with that in control fish fed a HCD. Body weight is considered to be tightly linked to metabolic pathways. When *insra* or *insrb* is deleted, insulin action is compromised in various physiological processes, especially those for glucose utilization. In our study, insulin signaling was

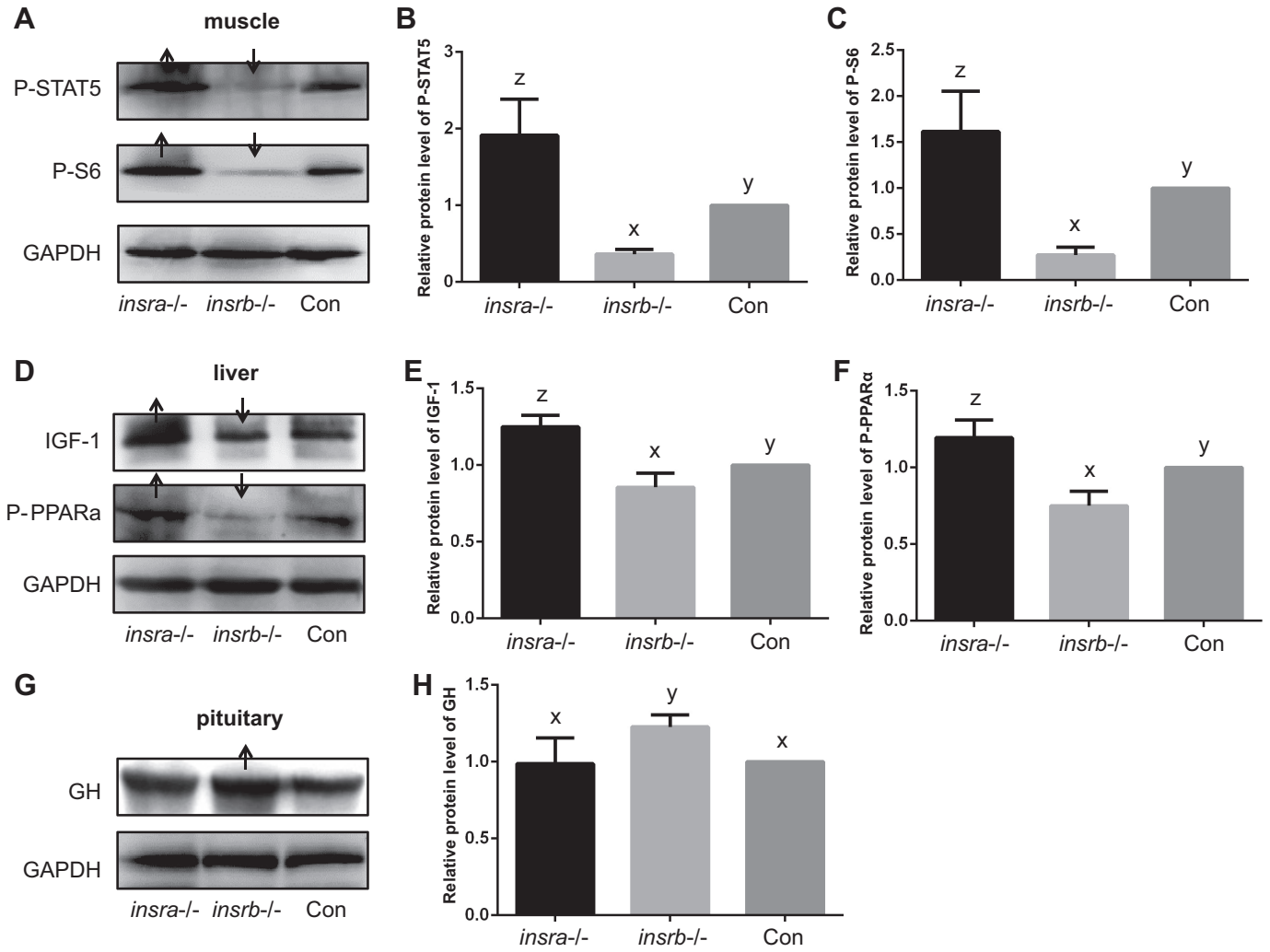

Fig. 5. Western blot analysis. *A*: P-STAT5 and P-S6 protein content in muscle samples of *insra*−/−, *insrb*−/−, and control fish. *B* and *C*: quantification of relative P-STAT5 and P-S6 protein levels from the Western blot are shown in *A*. *D*: insulin-like growth factor-1 (IGF-1) and P-PPARα protein content in liver samples of *insra*−/−, *insrb*−/−, and control fish. *E* and *F*: quantification of relative IGF-1 and P-PPARα protein levels from the Western blot are shown in *D*. *G*: growth hormone (GH) protein content in pituitary samples of *insra*−/−, *insrb*−/−, and control fish. *H*: quantification of relative GH protein level from the Western blot are shown in *G*. $n = 3$ for each genotype per time. All protein measurements were repeated 3 times independently. The letters *x*, *y*, and *z* in the bar chart represent significant differences of each index in *insra*−/− fish, *insrb*−/− fish, and control fish ($P < 0.05$). Red and green arrows indicate the upregulation and downregulation of proteins, respectively.

decreased significantly in *insra*−/− fish and *insrb*−/− fish, as proven by P-AKT and GCK protein levels and expression of *hkdc*, *gck*, *aldoaa*, and *pklr* (Fig. 1). In humans, impaired insulin action results in decreased insulin signaling in the hypothalamus, leading to increased food intake and weight gain (22). In the current study, food intake by *insra*−/− fish and *insrb*−/− fish was significantly higher than that of control fish. However, oxygen consumption in these two knockout genotypes was not changed compared with control fish. The increased food intake and unchanged oxygen consumption implied that more energy was retained in their bodies, leading to an increase in body weight in the mutants. In addition, AMPK is generally accepted as a crucial cellular energy sensor in maintaining energy homeostasis (35). When AMPK is inactivated, it switches off catabolic pathways that generate ATP but switches on biosynthetic pathways, such as biosynthesis of lipids, carbohydrates, and proteins that consume ATP (14). Meanwhile, it has been reported that a high glucose concentration can inhibit AMPK (56). In our study, *insra*−/− fish and *insrb*−/− fish exhibited a one- to twofold increase in prandial blood glucose level compared with control fish, which could inhibit AMPK signaling (Fig. 2). As a result, the increased food intake and activated biosynthetic process caused by decreased phosphorylation levels of AMPK in mutants actually led to increased body weight compared with the control siblings.

The liver plays a central role in maintaining body energy metabolism, while adipose tissue is responsible for energy storage (7). When lipids in the body exceed the amount the liver can handle, fat accumulates in the liver (31). In mammals, hepatic triacylglycerol is associated with insulin resistance. In obesity, some adipocyte-derived factors and products of macrophages are increased, resulting in insulin resistance by reducing PI3K signaling in muscles (22, 61). It has been proposed that increased NEFA levels and decreased intracellular content of fatty acids attenuate insulin/insr signaling (48, 49).

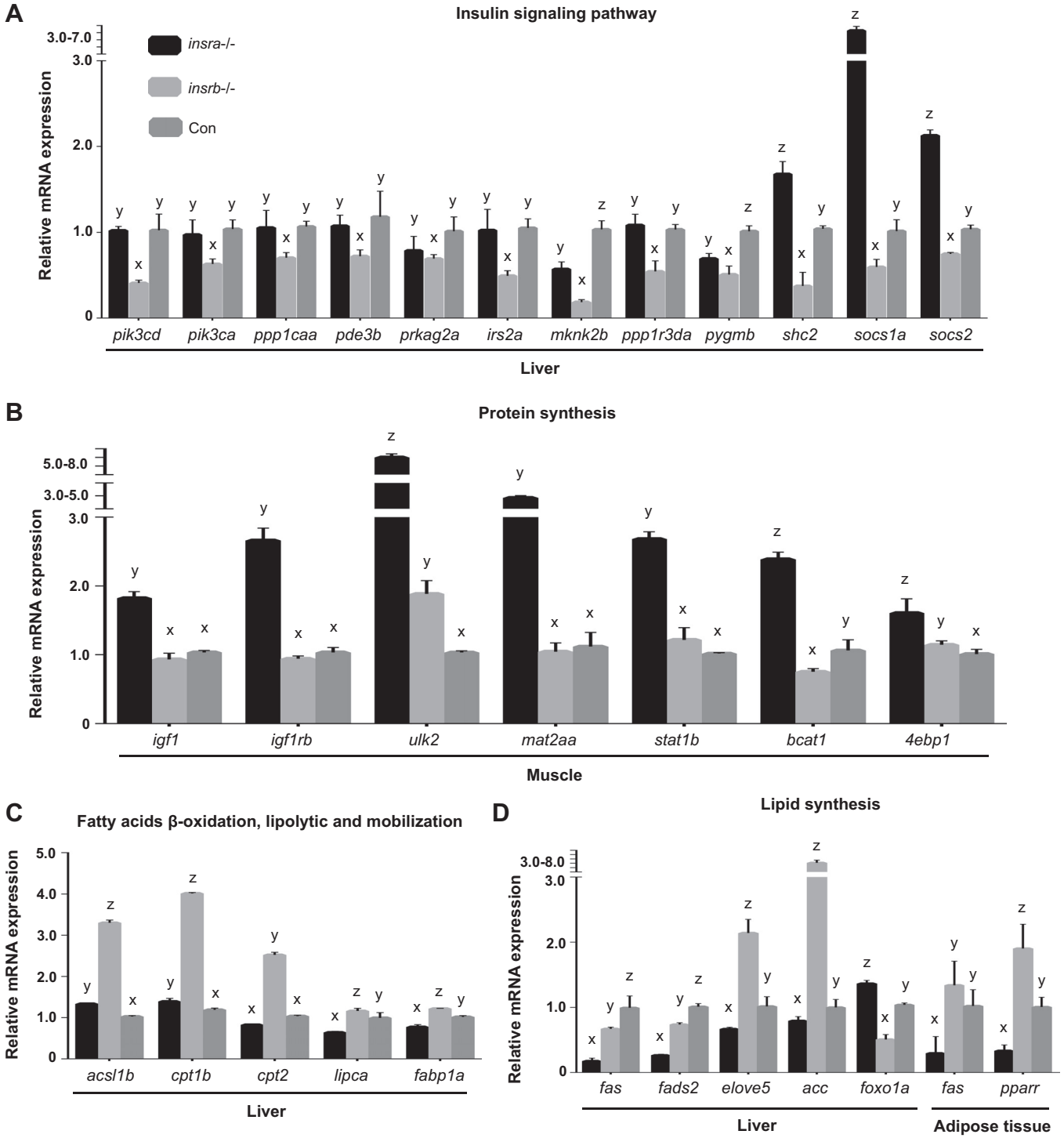

Fig. 6. Real-time quantitative PCR analysis of genes involved in the insulin signaling pathway, protein synthesis, lipid catabolism, and lipid synthesis. *A*: expression levels of *pik3cd, pik3ca*, *ppp1caa*, *pde3b*, *prkag2a*, *irs2a*, *mknk2b*, *ppp1r3da*, *pygmb*, *shc2*, *socs1a*, and *socs2* in liver samples of *insrb*−/− significantly decreased compared with control fish and *insra*−/− fish. *B*: expression levels of *igf1*, *igf1rb*, *ulk2*, *mat2aa*, *stat1b*, *bcat1*, and *4ebp1* in muscle samples of *insra*−/− fish significantly increased compared with control fish and *insrb*−/− fish. *C*: expression levels of *acs1b*, *cpt1b*, *cpt2*, *lipca*, and *fabp1a* in liver samples of *insrb*−/− fish significantly increased compared with control fish. *D*: expression levels of *fas*, *pparγ, fads2*, *elove5*, *acc*, and *foxo1a* in liver samples, and *fas* and *pparrγ* in adipose samples of *insra*−/− fish significantly affected compared with control fish. All mRNA measurements were repeated 3 times independently. The letters *x*, *y*, and *z* in the bar chart represent significant differences of each index in *insra*−/− fish, *insrb*−/− fish, and control fish ($P < 0.05$); $n = 3$ for each genotype per time.

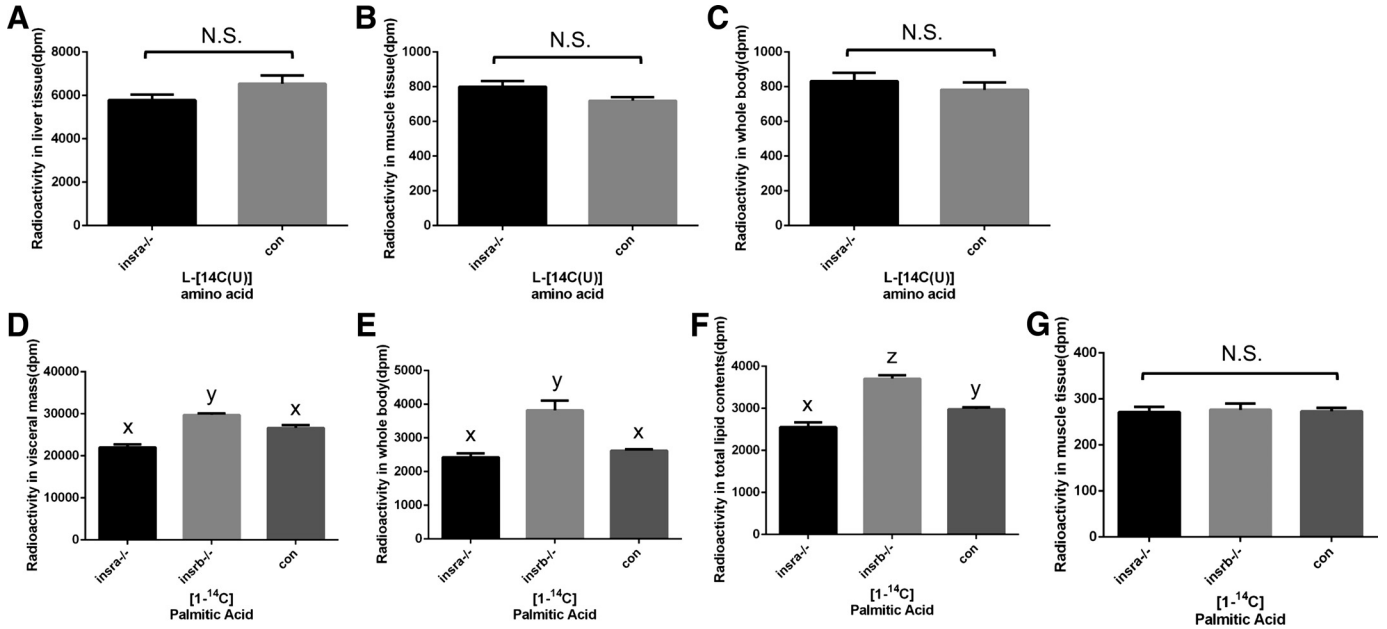

Fig. 7. Measurements of protein and lipid synthesis. *A–C*: measurement of the retention of radioactivity 2 h after intraperitoneal injection of L-[^{14} C(U)] amino acid mixture in zebrafish of 3 genotypes to examine the level of protein synthesis in liver, muscle, and the whole body ($n = 5$ for each genotype). *D–G*: measurement of the retention of radioactivity 2 h after intraperitoneal injection of palmitic acid [1-^{14}C] in zebrafish of 3 genotypes to examine the level of lipid synthesis in visceral mass, the whole body, lipid, and muscle ($n = 5$ for each genotype). The letters *x*, *y*, and *z* in the bar chart represent significant differences of each index in *insra*−/− fish, *insrb*−/− fish and control fish ($P < 0.05$). N. S., no significance.

This is consistent with the plasma lipid features observed in the *insrb*-deficiency group, which demonstrated increased NEFA, cholesterol, triglycerides, and phospholipids (Fig. 4). As described in a prior review (40, 55), insulin resistance may enhance hepatic fat accumulation by increasing free fatty acid delivery and inducing hyperinsulinemia to stimulate anabolic processes. Similarly, *insrb*−/− fish exhibited increased fatty acid delivery, as shown by upregulated expression of fatty acid binding protein (*fabp1a*) (Fig. 6). The diminished activation of P-PPARα and compromised GH-signaling pathway in *insrb*−/− fish livers, suggested that impaired hepatic triglycerides catabolism accounted for the fatty liver (Fig. 5). Furthermore, with no more than a 2% increase in carcass lipid content in *insrb*−/− fish, the fat in the current model of *insrb*−/− fish showed a specific increase in visceral tissues, without significant alterations in peripheral tissues (Fig. 3 and Table 4).

In mammals, GH/IGF-1 signaling regulates skeletal muscle growth (46). To test the status of GH/IGF-1 signaling in *insra*-deficient fish, the expression levels of *igf-1* and *igf-1r* and protein levels of IGF-1, P-STAT5, and P-S6 were examined. These results (Figs. 5 and 6), along with the increased level of overall crude body protein, suggest that GH/IGF-1 signaling is highly activated in *insra*−/− fish. This is also evidenced by upregulated *shc2*, *socs1a*, and *socs2* in the insulin-signaling pathway compared with the control fish. A decreased amount of visceral adipose tissue was observed in *insra*−/− fish (Table 4), which contrasted with the increased adipose tissue in *gh* mutant fish (36). This was also validated by the result that *insra*−/− fish had the lowest levels of plasma and hepatic TG, plasma NEFA, and plasma phospholipids (Fig. 4). This outcome is consistent with the composition measurements in *insra*−/− fish (Table 4), i.e., increased protein content and decreased lipid content. Combined with slightly higher retention of an amino acid mixture in muscle and whole body of *insra*−/− fish than control fish (Fig. 7, *A–C*), these results suggested that the activated GH signaling pathway, which promoted protein synthesis and lipid catabolism, was facilitated via Insrb when *insra* was depleted. Strong evidence suggests that insulin is required for the GH stimulation of hepatic IGF-1 production. Insulin-dependent diabetes mellitus is accompanied by GH resistance, with high GH levels in serum but low circulating IGF-1 levels and poor growth (17, 50, 52). These results indicate that insulin is necessary for the GH stimulation of IGF-1 production and growth. Animal studies have demonstrated that insulin increases total GH binding in the rat liver (3). However, the mechanisms involved in this process have not been extensively studied. Our present results provided more evidence for the positive regulatory function of insulin/insrb on GH signaling in zebrafish (Fig. 5). These findings support the results reported by Leung et al. (32), who demonstrated that insulin increases GH signaling by upregulating *ghr* mRNA abundance and total cellular content of immunoreactive and functional receptors in HuH7 cells.

Interestingly, the genes involved in lipogenesis, i.e., *fas*, *fads2*, *elovl5*, *acc*, and *foxo1a*, were uniformly downregulated in *insra*−/− fish (Fig. 6*C*), suggesting impaired lipogenesis in *insra*−/− fish. Combined with impaired glucose utilization, we hypothesize that the transition from glucose to lipids may be disrupted when insra is depleted. However, the downregulation of genes involved in lipogenesis was not observed in *insrb*−/− fish, except for the key molecule that inhibits lipogenesis but promotes lipolysis, *foxo1a* (41). Meanwhile, combined with the retention of fatty acids in the liver, whole body and total lipids were significant higher in *insrb*−/− fish ($P < 0.05$) than the other two groups. These results suggested that lipid synthesis was promoted in *insrb*−/− fish.

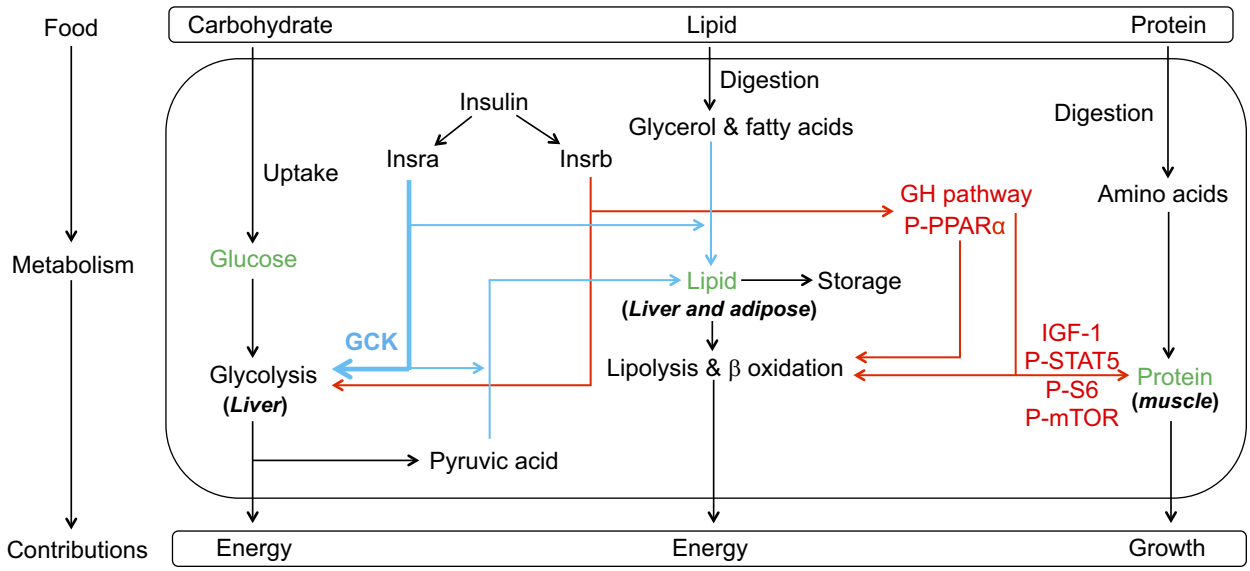

Fig. 8. Schematic model for the physiological roles of Insra and Insrb. In the present study, we demonstrated that, although Insra and Insrb share somewhat overlapping roles during glucose metabolism (blue and red lines), Insra promotes the transition of glucose to lipids (blue lines), while Insrb promotes lipid catabolism and protein synthesis by activating the growth hormone (GH) signaling pathway (red lines).

In our previous study, we performed RT-PCR of the two receptors of insulin and observed similar expression patterns, with both receptors abundantly expressed during early embryonic development and in tissues from adult fish (60). Uniformly, glucose levels increased in *insra*−/− fish and *insrb*−/− fish at both embryonic stage and adult stages, with *insra*−/− fish showing the highest level of glucose among the three genotypes. These results indicate that Insra plays a more important role in mediating glucose utilization. Combined with the increased glucose level and decreased lipid content in *insra*−/− fish, we speculate that insulin promotes the transition from glucose to lipids via Insra, rather than Insrb, in both liver and adipose tissues. Interestingly, the examination of key elements involved in the insulin signaling pathway demonstrated that these genes were largely unaffected in *insra*−/− fish compared with control fish. Together with overactivated GH signaling (increased *shc*, *socs1a*, *socs2*, *igf1*, and *igf1r*), these results suggest that Insrb mediates GH to regulate IGF-1/IGF-R signaling to compensate for the lack of insulin/insra signaling (10). It has been reported that receptors with intracellular domains of IGF1R show increased activation of Shc and Gab-1 and more potent regulation of genes involved in proliferation, corresponding to their higher mitogenic activity. Meanwhile, receptors with the intracellular domain of Insr display higher IRS-1 phosphorylation, stronger regulation of genes in metabolic pathways, and more dramatic glycolytic responses to hormonal stimulation (5). This may account for the increased GH/IGF-1 signaling and protein synthesis in *insra*−/− fish.

After the discovery of the duplicated *insr* genes, *insra* and *insrb* (54, 60), subsequent work has mainly focused on embryonic development. Although it is interesting to speculate whether *insr* isoforms may have different physiological roles, the effects on metabolism have not been well studied due to the lack of effective models. However, this situation is changing with the genetic editing approaches of TALEN and CRISPR/Cas9 (13, 19). Utilizing our recent *insra*−/− and *insrb*−/− models, we are able to investigate the precise functions of Insra and Insrb on zebrafish nutrient metabolism and somatic growth. Dysfunction of insulin receptors and components of the downstream signaling cascade results in insulin resistance, which leads to type 2 diabetes mellitus. Mutations in insulin receptors can result in many syndromes, such as leprechaunism and Rabson-Mendenhall syndrome. Uniformly, patients with these syndromes demonstrate severe insulin resistance (53). Although clinical data indicate that insulin receptors are essential for development and metabolism, the mechanisms involved in nutrient metabolism, which could provide evidence for the treatment of these syndromes, are less defined. Thus, in utilizing the *insra* and *insrb* knockout zebrafish with a high-carbohydrate diet as the model, this study provides a system to understand the physiological roles of Insra or Insrb. Using this system, we show that both Insra and Insrb play important roles in maintaining the transduction of insulin signaling and glycolysis, but Insra mainly promotes the transition from glucose to lipids, whereas Insrb acts to promote lipid catabolism and protein synthesis by enhancing the GH signaling pathway (Fig. 8).

GRANTS

This work was supported by the National Basic Research Program of China (2014CB138602), Youth Innovation Promotion Association of Chinese Academy of Science (2013223), National Natural Science Foundation of China (31672670), the Chinese Academy of Sciences (XDA08010405), China Agriculture Research System (CARS-46-18), and Fund Project in State Key Laboratory of Freshwater Ecology and Biotechnology (2016FBZ05).

DISCLOSURES

No conflicts of interest, financial or otherwise, are declared by the authors.

AUTHOR CONTRIBUTIONS

D.H. conceived and designed research; B.-Y.Y., G.Z., Y.-L.G., and J.-Z.S. performed experiments; B.-Y.Y., G.Z., Y.-L.G., J.-Z.S., X.-Y.P., G.-H.S., D.H., and J.-Y.J. analyzed data; B.-Y.Y., G.Z., Y.-L.G., J.-Z.S., X.-Y.P., G.-H.S., D.H., J.-Y.J., and H.-K.L. interpreted results of experiments; B.-Y.Y. and G.Z. drafted manuscript; B.-Y.Y., D.H., Z.-Y.D., Z.Y., and S.-Q.X. edited

and revised manuscript; B.-Y.Y. approved final version of manuscript; G.Z. and H.-K.L. prepared figures.

REFERENCES

1. **Accili D, Drago J, Lee EJ, Johnson MD, Cool MH, Salvatore P, Asico LD, José PA, Taylor SI, Westphal H.** Early neonatal death in mice homozygous for a null allele of the insulin receptor gene. *Nat Genet* 12: 106–109, 1996. doi:10.1038/ng0196-106.
2. **Avruch J.** Insulin signal transduction through protein kinase cascades. *Mol Cell Biochem* 182: 31–48, 1998. doi:10.1023/A:1006823109415.
3. **Baxter RC, Bryson JM, Turtle JR.** Somatogenic receptors of rat liver: regulation by insulin. *Endocrinology* 107: 1176–1181, 1980. doi:10.1210/endo-107-4-1176.
4. **Bustin SA, Benes V, Garson JA, Hellemans J, Huggett J, Kubista M, Mueller R, Nolan T, Pfaffl MW, Shipley GL, Vandesompele J, Wittwer CT.** The MIQE guidelines: minimum information for publication of quantitative real-time PCR experiments. *Clin Chem* 55: 611–622, 2009. doi:10.1373/clinchem.2008.112797.
5. **Cai W, Sakaguchi M, Kleinridders A, Gonzalez-Del Pino G, Dreyfuss JM, O'Neill BT, Ramirez AK, Pan H, Winnay JN, Boucher J, Eck MJ, Kahn CR.** Domain-dependent effects of insulin and IGF-1 receptors on signalling and gene expression. *Nat Commun* 8: 14892, 2017. doi:10.1038/ncomms14892.
6. **Cho H, Mu J, Kim JK, Thorvaldsen JL, Chu Q, Crenshaw EB 3rd, Kaestner KH, Bartolomei MS, Shulman GI, Birnbaum MJ.** Insulin resistance and a diabetes mellitus-like syndrome in mice lacking the protein kinase Akt2 (PKB beta). *Science* 292: 1728–1731, 2001. doi:10.1126/science.292.5522.1728.
7. **Dai Z, Wang H, Jin X, Wang H, He J, Liu M, Yin Z, Sun Y, Lou Q.** Depletion of suppressor of cytokine signaling-1a causes hepatic steatosis and insulin resistance in zebrafish. *Am J Physiol Endocrinol Metab* 308: E849–E859, 2015. doi:10.1152/ajpendo.00540.2014.
8. **Dimitriadis G, Mitrou P, Lambadiari V, Maratou E, Raptis SA.** Insulin effects in muscle and adipose tissue. *Diabetes Res Clin Pract* 93, *Suppl* 1: S52–S59, 2011. doi:10.1016/S0168-8227(11)70014-6.
9. **Duan C, Ren H, Gao S.** Insulin-like growth factors (IGFs), IGF receptors, and IGF-binding proteins: roles in skeletal muscle growth and differentiation. *Gen Comp Endocrinol* 167: 344–351, 2010. doi:10.1016/j.ygcen.2010.04.009.
10. **Entingh-Pearsall A, Kahn CR.** Differential roles of the insulin and insulin-like growth factor-I (IGF-I) receptors in response to insulin and IGF-I. *J Biol Chem* 279: 38016–38024, 2004. doi:10.1074/jbc.M313201200.
11. **Falik Zaccai TC, Kalfon L, Klar A, Elisha MB, Hurvitz H, Weingarten G, Chechik E, Fleisher Sheffer V, Haj Yahya R, Meidan G, Gross-Kieselstein E, Bauman D, Hershkovitz S, Yaron Y, Orr-Urtreger A, Wertheimer E.** Two novel mutations identified in familial cases with Donohue syndrome. *Mol Genet Genomic Med* 2: 64–72, 2014. doi:10.1002/mgg3.43.
12. **Folch J, Lees M, Sloane Stanley GH.** A simple method for the isolation and purification of total lipides from animal tissues. *J Biol Chem* 226: 497–509, 1957.
13. **Gaj T, Gersbach CA, Barbas CF 3rd.** ZFN, TALEN, and CRISPR/Cas-based methods for genome engineering. *Trends Biotechnol* 31: 397–405, 2013. doi:10.1016/j.tibtech.2013.04.004.
14. **Hardie DG, Ross FA, Hawley SA.** AMPK: a nutrient and energy sensor that maintains energy homeostasis. *Nat Rev Mol Cell Biol* 13: 251–262, 2012. doi:10.1038/nrm3311.
15. **Hayashi AA, Proud CG.** The rapid activation of protein synthesis by growth hormone requires signaling through mTOR. *Am J Physiol Endocrinol Metab* 292: E1647–E1655, 2007. doi:10.1152/ajpendo.00674.2006.
16. **Hernández-Sánchez C, Mansilla A, de la Rosa EJ, de Pablo F.** Proinsulin in development: New roles for an ancient prohormone. *Diabetologia* 49: 1142–1150, 2006. doi:10.1007/s00125-006-0232-5.
17. **Horner JM, Kemp SF, Hintz RL.** Growth hormone and somatomedin in insulin-dependent diabetes mellitus. *J Clin Endocrinol Metab* 53: 1148–1153, 1981. doi:10.1210/jcem-53-6-1148.
18. **Horwitz W.** Official methods of analysis of the association of official analytical chemists. *J Pharm Sci* 60: 916, 1984.
19. **Huang P, Xiao A, Zhou M, Zhu Z, Lin S, Zhang B.** Heritable gene targeting in zebrafish using customized TALENs. *Nat Biotechnol* 29: 699–700, 2011. doi:10.1038/nbt.1939.
20. **Hubbard SR.** Crystal structure of the activated insulin receptor tyrosine kinase in complex with peptide substrate and ATP analog. *EMBO J* 16: 5572–5581, 1997. doi:10.1093/emboj/16.18.5572.
21. **Joshi RL, Lamothe B, Cordonnier N, Mesbah K, Monthioux E, Jami J, Bucchini D.** Targeted disruption of the insulin receptor gene in the mouse results in neonatal lethality. *EMBO J* 15: 1542–1547, 1996.
22. **Kahn SE, Hull RL, Utzschneider KM.** Mechanisms linking obesity to insulin resistance and type 2 diabetes. *Nature* 444: 840–846, 2006. doi:10.1038/nature05482.
24. **Kane S, Sano H, Liu SC, Asara JM, Lane WS, Garner CC, Lienhard GE.** A method to identify serine kinase substrates. Akt phosphorylates a novel adipocyte protein with a Rab GTPase-activating protein (GAP) domain. *J Biol Chem* 277: 22115–22118, 2002. doi:10.1074/jbc.C200198200.
25. **Kaushik S, Georga I, Koumoundouros G.** Growth and body composition of zebrafish (Danio rerio) larvae fed a compound feed from first feeding onward: toward implications on nutrient requirements. *Zebrafish* 8: 87–95, 2011. doi:10.1089/zeb.2011.0696.
26. **Kawai M, Namba N, Mushiake S, Etani Y, Nishimura R, Makishima M, Ozono K.** Growth hormone stimulates adipogenesis of 3T3-L1 cells through activation of the Stat5A/5B-PPARgamma pathway. *J Mol Endocrinol* 38: 19–34, 2007. doi:10.1677/jme.1.02154.
27. **Kim YD, Li T, Ahn SW, Kim DK, Lee JM, Hwang SL, Kim YH, Lee CH, Lee IK, Chiang JY, Choi HS.** Orphan nuclear receptor small heterodimer partner negatively regulates growth hormone-mediated induction of hepatic gluconeogenesis through inhibition of signal transducer and activator of transcription 5 (STAT5) transactivation. *J Biol Chem* 287: 37098–37108, 2012. doi:10.1074/jbc.M112.339887.
28. **Kitamura T, Kahn CR, Accili D.** Insulin receptor knockout mice. *Annu Rev Physiol* 65: 313–332, 2003. doi:10.1146/annurev.physiol.65.092101.142540.
29. **Lanning NJ, Carter-Su C.** Recent advances in growth hormone signaling. *Rev Endocr Metab Disord* 7: 225–235, 2006. doi:10.1007/s11154-007-9025-5.
30. **Laplante M, Sabatini DM.** An emerging role of mTOR in lipid biosynthesis. *Curr Biol* 19: R1046–R1052, 2009. doi:10.1016/j.cub.2009.09.058.
31. **Lebovics E, Rubin J.** Non-alcoholic fatty liver disease (NAFLD): why you should care, when you should worry, what you should do. *Diabetes Metab Res Rev* 27: 419–424, 2011. doi:10.1002/dmrr.1198.
32. **Leung KC, Doyle N, Ballesteros M, Waters MJ, Ho KK.** Insulin regulation of human hepatic growth hormone receptors: divergent effects on biosynthesis and surface translocation. *J Clin Endocrinol Metab* 85: 4712–4720, 2000. doi:10.1210/jcem.85.12.7017.
33. **Leung KC, Ho KK.** Stimulation of mitochondrial fatty acid oxidation by growth hormone in human fibroblasts. *J Clin Endocrinol Metab* 82: 4208–4213, 1997. doi:10.1210/jcem.82.12.4459.
34. **Li D, Lou Q, Zhai G, Peng X, Cheng X, Dai X, Zhuo Z, Shang G, Jin X, Chen X, Han D, He J, Yin Z.** Hyperplasia and cellularity changes in IGF-1-overexpressing skeletal muscle of crucian carp. *Endocrinology* 155: 2199–2212, 2014. doi:10.1210/en.2013-1938.
35. **Lim CT, Kola B, Korbonits M.** AMPK as a mediator of hormonal signalling. *J Mol Endocrinol* 44: 87–97, 2010. doi:10.1677/JME-09-0063.
36. **McMenamin SK, Minchin JE, Gordon TN, Rawls JF, Parichy DM.** Dwarfism and increased adiposity in the gh1 mutant zebrafish vizzini. *Endocrinology* 154: 1476–1487, 2013. doi:10.1210/en.2012-1734.
37. **De Meyts P, Whittaker J.** Structural biology of insulin and IGF1 receptors: implications for drug design. *Nat Rev Drug Discov* 1: 769–783, 2002. doi:10.1038/nrd917.
38. **Mihaylova MM, Shaw RJ.** The AMPK signalling pathway coordinates cell growth, autophagy and metabolism. *Nat Cell Biol* 13: 1016–1023, 2011. doi:10.1038/ncb2329.
39. **Møller N, Gjedsted J, Gormsen L, Fuglsang J, Djurhuus C.** Effects of growth hormone on lipid metabolism in humans. *Growth Horm IGF Res* 13, *Suppl A*: S18–S21, 2003. doi:10.1016/S1096-6374(03)00048-0.
40. **Nagle CA, Klett EL, Coleman RA.** Hepatic triacylglycerol accumulation and insulin resistance. *J Lipid Res* 50, *Suppl*: S74–S79, 2009. doi:10.1194/jlr.R800053-JLR200.
41. **Nakae J, Biggs WH 3rd, Kitamura T, Cavenee WK, Wright CV, Arden KC, Accili D.** Regulation of insulin action and pancreatic beta-cell function by mutated alleles of the gene encoding forkhead transcription factor Foxo1. *Nat Genet* 32: 245–253, 2002. doi:10.1038/ng890.
42. **Ning LJ, He AY, Lu DL, Li JM, Qiao F, Li DL, Zhang ML, Chen LQ, Du ZY.** Nutritional background changes the hypolipidemic effects of fenofibrate in Nile tilapia (Oreochromis niloticus). *Sci Rep* 7: 41706, 2017. doi:10.1038/srep41706.
43. **Rocha F, Dias J, Engrola S, Gavaia P, Geurden I, Dinis MT, Panserat S.** Glucose metabolism and gene expression in juvenile zebrafish (Danio

rerio) challenged with a high carbohydrate diet: effects of an acute glucose stimulus during late embryonic life. *Br J Nutr* 113: 403–413, 2015. doi:10.1017/S0007114514003869.
44. **Rui L.** Energy metabolism in the liver. *Compr Physiol* 4: 177–197, 2014. doi:10.1002/cphy.c130024.
45. **Saltiel AR, Kahn CR.** Insulin signalling and the regulation of glucose and lipid metabolism. *Nature* 414: 799–806, 2001. doi:10.1038/414799a.
46. **Schiaffino S, Mammucari C.** Regulation of skeletal muscle growth by the IGF1-Akt/PKB pathway: insights from genetic models. *Skelet Muscle* 1: 4, 2011. doi:10.1186/2044-5040-1-4.
47. **Shalev A, Siegrist-Kaiser CA, Yen PM, Wahli W, Burger AG, Chin WW, Meier CA.** The peroxisome proliferator-activated receptor alpha is a phosphoprotein: regulation by insulin. *Endocrinology* 137: 4499–4502, 1996. doi:10.1210/endo.137.10.8828512.
48. **Shulman GI.** Cellular mechanisms of insulin resistance. *J Clin Invest* 106: 171–176, 2000. doi:10.1172/JCI10583.
49. **Shulman GI.** Cellular mechanisms of insulin resistance in humans. *Am J Cardiol* 84, *1A*: 3J–10J, 1999. doi:10.1016/S0002-9149(99)00350-1.
50. **Tan K, Baxter RC.** Serum insulin-like growth factor I levels in adult diabetic patients: the effect of age. *J Clin Endocrinol Metab* 63: 651–655, 1986. doi:10.1210/jcem-63-3-651.
51. **Taniguchi CM, Emanuelli B, Kahn CR.** Critical nodes in signalling pathways: insights into insulin action. *Nat Rev Mol Cell Biol* 7: 85–96, 2006. doi:10.1038/nrm1837.
52. **Tattersall RB, Pyke DA.** Growth in diabetic children. Studies in identical twins. *Lancet* 2: 1105–1109, 1973. doi:10.1016/S0140-6736(73)90931-8.
53. **Taylor SI, Arioglu E.** Genetically defined forms of diabetes in children. *J Clin Endocrinol Metab* 84: 4390–4396, 1999. doi:10.1210/jcem.84.12.6237.
54. **Toyoshima Y, Monson C, Duan C, Wu Y, Gao C, Yakar S, Sadler KC, LeRoith D.** The role of insulin receptor signaling in zebrafish embryogenesis. *Endocrinology* 149: 5996–6005, 2008. doi:10.1210/en.2008-0329.
55. **Utzschneider KM, Kahn SE.** Review: The role of insulin resistance in nonalcoholic fatty liver disease. *J Clin Endocrinol Metab* 91: 4753–4761, 2006. doi:10.1210/jc.2006-0587.
56. **Viollet B, Horman S, Leclerc J, Lantier L, Foretz M, Billaud M, Giri S, Andreelli F.** AMPK inhibition in health and disease. *Crit Rev Biochem Mol Biol* 45: 276–295, 2010. doi:10.3109/10409238.2010.488215.
57. **Walsh PT, Smith LM, O'Connor R.** Insulin-like growth factor-1 activates Akt and Jun N-terminal kinases (JNKs) in promoting the survival of T lymphocytes. *Immunology* 107: 461–471, 2002. doi:10.1046/j.1365-2567.2002.01525.x.
58. **Wertheimer E, Lu SP, Backeljauw PF, Davenport ML, Taylor SI.** Homozygous deletion of the human insulin receptor gene results in leprechaunism. *Nat Genet* 5: 71–73, 1993. doi:10.1038/ng0993-71.
59. **Westerfield M.** *The Zebrafish Book, A Guide For The Laboratory Use Of Zebrafish (Danio Rerio)*. (4th ed.). Eugene, OR: Univ. of Oregon, 2000.
60. **Yang BY, Zhai G, Gong YL, Su JZ, Han D, Yin Z, Xie SQ.** Depletion of insulin receptors leads to beta-cell hyperplasia in zebrafish. *Sci Bull (Beijing)* 62: 486–492, 2017. doi:10.1016/j.scib.2017.03.001.
61. **Yang Q, Graham TE, Mody N, Preitner F, Peroni OD, Zabolotny JM, Kotani K, Quadro L, Kahn BB.** Serum retinol binding protein 4 contributes to insulin resistance in obesity and type 2 diabetes. *Nature* 436: 356–362, 2005. doi:10.1038/nature03711.
62. **Zhang D, Wang J, Zhou C, Xiao W.** Zebrafish akt2 is essential for survival, growth, bone development, and glucose homeostasis. *Mech Dev* 143: 42–52, 2017. doi:10.1016/j.mod.2017.01.004.
63. **Zheng WH, Quirion R.** Insulin-like growth factor-1 (IGF-1) induces the activation/phosphorylation of Akt kinase and cAMP response element-binding protein (CREB) by activating different signaling pathways in PC12 cells. *BMC Neurosci* 7: 51, 2006. doi:10.1186/1471-2202-7-51.